Article

In-silico and *in-vitro* screening for P-glycoprotein interaction with tenofovir, darunavir and dapivirine: an anti-retroviral drug combination for topical prevention of colorectal HIV transmission

Magda Swedrowska, Shirin Jamshidi, Abhinav Kumar, Charles Kelly, K. Miraz Rahman, and Ben Forbes

Mol. Pharmaceutics, **Just Accepted Manuscript** • DOI: 10.1021/acs.molpharmaceut.7b00133 • Publication Date (Web): 25 Jun 2017

In-silico and *in-vitro* screening for P-glycoprotein interaction with tenofovir, darunavir and dapivirine: an anti-retroviral drug combination for topical prevention of colorectal HIV transmission

Magda Swedrowska[1], Shirin Jamshidi[1], Abhinav Kumar[1], Charles Kelly[2], K. Miraz Rahman[1], Ben Forbes[1*].

1. **Institute of Pharmaceutical Science, King's College London, London, SE1 9NH, UK**
2. **Oral Immunology, King's College London, London, UK**

*** Corresponding Author**

Prof. Ben Forbes

Institute of Pharmaceutical Science

King's College London,

150 Stamford Street, London, UK, SE1 9NH

Tel. +44 (0) 207 848 4823

E-mail: ben.forbes@kcl.ac.uk

Abstract

The aim of the study was to use *in-silico* and *in-vitro* techniques to evaluate whether a triple formulation of antiretroviral drugs (tenofovir, darunavir and dapivirine) interacted with p-glycoprotein (P-gp) or exhibited any other permeability-altering drug-drug interactions in the colorectal mucosa.

Potential drug interactions with P-gp were screened initially using molecular docking, followed by molecular dynamics simulations to analyse the identified drug-transporter interaction more mechanistically. The transport of tenofovir, darunavir and dapivirine was investigated in the Caco-2 cells models and colorectal tissue and their apparent permeability coefficient (P_{app}), efflux ratio (ER) and the effect of transporter inhibitors were evaluated.

In-silico, dapivirine and darunavir showed strong affinity for P-gp with similar free energy of binding; dapivirine exhibiting a ΔG_{PB} value -38.24 kcal/mol, darunavir with a ΔG_{PB} value -36.84 kcal/mol. The rank order of permeability of the compounds *in-vitro* was tenofovir < darunavir < dapivirine. The P_{app} for tenofovir in Caco-2 cell monolayers was $0.10 \pm 0.02 \times 10^{-6}$ cm/s, ER=1. For dapivirine, P_{app} was $32.2 \pm 3.7 \times 10^{-6}$ cm/s, but the ER=1.3 was lower than anticipated based on the *in-silico* findings. Neither tenofovir nor dapivirine transport was influenced by P-gp inhibitors. The absorptive permeability of darunavir ($P_{app}=6.4 \pm 0.9 \times 10^{-6}$ cm/s) was concentration dependent with ER=6.3, which was reduced by verapamil to 1.2. Administration of the drugs in combination did not alter their permeability compared to administration as single agents.

In conclusion, *in-silico* modelling, cell culture and tissue-based assays showed that tenofovir does not interact with P-gp and is poorly permeable, consistent with a paracellular transport mechanism. *In-silico* modelling predicted that darunavir and dapivirine were P-gp substrates, but only darunavir showed P-gp-dependent permeability in the biological models, illustrating that *in-silico* modelling requires experimental validation. When administered in combination, the disposition of the

proposed triple-therapy antiretroviral drugs in the colorectal mucosa will depend on their distinctly different permeability, but was not interdependent.

Key words: drug transporters; tenofovir; darunavir and dapivirine; *in-silico,* molecular dynamics simulation; intestinal permeability

Abbreviations:

ABC	ATP binding cassette
ARV	antiretroviral drug
BCRP	breast cancer resistance protein
HAART	highly active antiretroviral therapy
HIV	human immunodeficiency virus
MRP	multidrug resistance-associated protein
NNRTI	non-nucleoside reverse transcriptase inhibitor
NRTI	nucleoside/nucleotide reverse transcriptase inhibitor
P-gp	P-glycoprotein
PI	HIV-1 protease inhibitor
RAI	receptive anal intercourse

1. Introduction

Microbicides are compounds intended to prevent or significantly reduce the sexual transmission of the human immunodeficiency virus (HIV) infection. To date, the development of safe and efficient microbicides has largely focused on the product's design to prevent vaginal transmission of HIV [1]. However, the risk of HIV transmission during receptive anal intercourse (RAI) is about 18-fold greater than during vaginal intercourse [2], [3]. In contrast to the multiple layers of stratified squamous epithelium present in the female genital tract, the rectal mucosa has a single layer of columnar epithelium which separates lumen from the lamina propria and can be easily damaged during RAI [4]. Microbicide formulations applied topically in the rectum containing single anti-retroviral drugs (ARV) which prevent main stages in HIV replication; such as protease inhibitors, non-nucleoside reverse transcriptase inhibitors and entry inhibitors, have shown promising results in clinical trials [5].

Formulations based on single ARV drugs are susceptible to the increasing problem of drug-resistant HIV strains. Around 10-20% of new infections in the developed world are caused by strains resistant to at least one of three main classes of ARV. Combinations of two or more ARV drugs with different mechanisms of action are likely to be more effective against resistant strains and reduce viral load [6]. To date, only a few combination ARV microbicide formulations have been reported; these include ring formulations (dapivirine + maraviroc, dapivirine + tenofovir) and gel formulations (tenofovir + UC781, tenofovir + IQP-0528) [7], [8]. Furthermore, the dual combination of tenofovir and dapivirine was more active in inhibiting the replication of the HIV isolates than any of the individual compound in both cellular and tissues model [1]. Combination of tenofovir and UC781 led to a 61% reduction in the IC_{50} of tenofovir and a 50% reduction in the IC_{50} of UC781, suggesting that this combination is more potent than each agent alone [9]. As an extension of this approach, a novel microbicide formulation containing different classes of ARV, tenofovir, dapivirine and darunavir, is currently under investigation [10].

Tenofovir and dapivirine are nucleotide reverse transcriptase inhibitor and nonnucleoside reverse transcriptase inhibitor, respectively. Tenofovir is one of the most extensively studied microbicides [11]. Currently, it is licensed for oral use in the form of the prodrug tenofovir disoproxil fumarate, which is recommended as the first-line therapy for the treatment of HIV [12]. Dapivirine is undergoing phase III clinical trials in Africa as an intravaginal ring for use in HIV pre-exposure prophylaxis [13], [14], [15]. Darunavir is a nonpeptidic protease inhibitor, approved in 2006 for the treatment of drug-resistance HIV [16].

Most of the studies investigating these drugs as topical microbicides are focused on formulations for vaginal application [10]. Thus, the pharmacokinetics of ARVs following topical administration to the colorectal epithelium mucosa are unknown. Local drug concentrations determine efficacy and we hypothesise that these will depend on the level of expression of drug transporters in the colorectal epithelium. The colorectal epithelium is a tight epithelial monolayer and colorectal biopsies show the expression of ABC transporters such as P-gp, breast cancer resistance proteins (BCRP) and multidrug resistance proteins (MRPs, most probably MRP3) and several solute carrier transporters CNT2, CNT3, ENT2 and MCT1 [17] [18]. ABC transporters present at the apical membrane of colorectal tissue can mediate drug efflux into the lumen, significantly reducing the concentration-time profiles of ARV drugs in the tissue [19].

A variety of *in-silico* and *in-vitro* methods are available for studying the biopharmaceutics of drugs in the non-clinical phases of medicines development [20], [21]. Permeability models can help to eliminate or significantly reduce the risk of failure due to poor pharmacokinetics or drug-drug interactions in the late stage of drug development. In the present study, we performed molecular docking and MD simulations to screen for molecular interactions of tenofovir, dapivirine and darunavir with the P-gp transporter. Cell and tissue models of the colorectal epithelium were used to measure individual drug permeabilities and the effect of p-gp on tenofovir, dapivirine and darunavir transport was

evaluated along with any co-dependency in the permeability of drugs when measured in combination.

2. Materials and Methods

Materials

Caco-2 cells (human adenocarcinoma cell line) were purchased from the American Type Tissue Culture (ATCC, Rockville, USA). Hank's Balanced Salt Solution (HBSS), Dulbecco's modified Eagle's medium (DMEM), foetal bovine serum (FBS), non-essential amino acids, L-glutamine, penicillin/streptomycin, 4-(2-hydroxyethyl)-1-piperazineethanesulfonic acid (HEPES), poloxamer 407, CsA, haloperidol, verapamil, GF120918 and dimethyl sulfoxide (DMSO) were obtained from Sigma-Aldrich (Gillingham, UK). Transwell® 12-well plates (1.13 cm^2, 0.4 µm pore size, polycarbonate membrane) were purchased from Corning Costar Corporation (Cambridge, USA). Tenofovir was provided by Gilead Sciences (Foster City, USA), darunavir was provided by Janssen R&D Ireland (Cork, Ireland) and dapivirine was purchased from Selleckchem (Suffolk, UK). [^{14}C]-dapivirine, [^{14}C]-darunavir and [^{14}C]-tenofovir were purchased from Moravek Biochemicals (USA). [^{3}H]-mannitol, [^{14}C]-mannitol and [^{3}H]-digoxin were purchased from Perkin Elmer (Wokingham, UK).

Molecular docking

Coordinates of the P-gp efflux pump were obtained from the P-gp crystal structure from *Mus Musculus* (PDB ID 3G61, 4.35 Å resolution), reported by Aller S.G. et al [22]. The ligands were generated by Chem3D 15.0 software. All the structures were minimised using the AMBER 12.0 package program. Molecular docking protocols were used in order to predict the binding site and affinities for a number of ligands. The relationship between the binding affinity of the ligands and the docking score was used for the comparison of the binding energies and affinities of all the diverse ligands to the P-gp efflux pump. Molecular docking was performed to generate several distinct binding orientations and binding affinities for each binding mode. Subsequently, the binding modes that showed the lowest binding free energy were considered as the most favourable binding modes.

AutoDock SMINA was used for the molecular docking of the ligands to the efflux pump structures to find the best binding pocket by exploring all probable binding cavities in the protein. Then, the GOLD molecular docking method was applied for the docking of the ligands into the SMINA-located best binding site, for performing flexible molecular docking and determining more precise and evaluated energies and scores. Based on the fitness function scores and ligand binding positions, the best-docked poses for each ligand were selected. The fitness function score of poses, generated using the GOLD program that has the highest GOLD fitness score reveals the best-docked pose for each system, and was determined by analysing the fitness function score of poses (GOLD fitness energy) which was generated using the GOLD docking program.

The Genetic algorithm (GA) is used in GOLD ligand docking to examine the ligand conformational flexibility along with the partial flexibility of the protein [23]. The maximum number of runs was set to 20 for each compound and the default parameters were selected (100 population size, 5 for the number of islands, 100,000 number of operations and 2 for the niche size). Default cut off values of 2.5Å (dH-X) for hydrogen bonds and 4.0 Å for van-der-Waals distance were used. When the systems attained RMSD values within 1.5 Å, GA docking was terminated.

Molecular dynamics (MD) simulation

The best poses of mannitol, digoxin, tenofovir, dapivirine and darunavir located in transmembrane domains of P-gp efflux pump were selected to provide the corresponding complex of each ligand with P-gp to run MD simulations combined with MM-PBSA/MM-GBSA calculation. A simulation for ligand-free P-gp was run as a control. All the MD simulations were carried out using the AMBER 12.0 package. Each system was solvated using an octahedral box of TIP3P water molecules. Periodic boundary conditions and the particle-mesh Ewald (PME) method were employed in all of the simulations [24]. During each simulation, all bonds in which the hydrogen atom was present were considered fixed and all other bonds were constrained to their equilibrium values by applying

the SHAKE algorithm [25] . The force fields parameters for the ligands were generated by using the ANTECHAMBER module of the AMBER program.

A cut off radius of 12 Å was used for the ligand-free proteins and complexes. Each of two minimization phases were performed in two stages. In the first phase, ions and all water molecules were minimized for 500 cycles of steepest descent followed by 500 cycles of conjugate gradient minimization. Afterward, the systems were minimized for a total of 2500 cycles without restraint wherein 1000 cycles of steepest descent were followed by 1500 cycles of conjugate gradient minimization. After minimisations, the systems were heated for 500 ps while the temperature was raised from 0 to 300 K, and then equilibration was performed without a restraint for 100 ps while the temperature was kept at 300 K. Sampling of reasonable configurations was conducted by running a 50 ns simulation with a 2 fs time step at 300 K and 1 atm pressure. A constant temperature was maintained by applying the Langevin algorithm, while the pressure was controlled by the isotropic position scaling protocol used in AMBER [26]. All histidines were protonated at their δ-nitrogen atoms.

To perform MM-PBSA/MM-GBSA calculations, 10 snapshots were collected from the last 100 ps of simulations of protein-ligand complexes for post-processing analysis. The gas-phase interaction energy between the protein and the ligand ΔE_{MM} was the sum of electrostatic and van der Waals interaction energies. The solvation free energy ΔG_{sol} was the sum of the polar (ΔG_{PB}) and non-polar (ΔG_{SA}) parts. The ΔG_{PB} term was calculated by solving the finite-difference Poisson-Boltzmann equation using the internal PBSA program. The SCALE value was set to 5. The Parse radii were employed for all atoms [27]. The solvent probe radius was set at 1.4 Å (with the radii in the prm top files). MM-PBSA calculation was performed with the PBSA module (PROC=2). The value of the exterior dielectric constant was set at 80, and the solute dielectric constant was set at 1 [28]. The nonpolar contribution was determined on the basis of the solvent accessible surface area (SASA) using the LCPO method [29], ΔG_{SA}=0.04356×ΔSASA and CAVITY-OFFSET set at -1.008.

In the MM-GBSA calculations, like the MM-PBSA calculations, the gas-phase interaction energy (ΔE_{MM}) and the non-polar (ΔG_{SA}) part of the solvation energy were calculated. The electrostatic solvation energy in ΔG_{GB} was calculated by using GB models [30]. A value of 80 was used for the exterior dielectric constant, and a value of 1 was used for the solute dielectric constant for comparison. The binding free energies were calculated by using both the MM-PBSA and the MM-GBSA methods.

Caco-2 cell culture

Caco-2 cells were grown in 162 cm^2 cell culture flasks at 37˚C in 95% air, 5% CO_2. The cells were cultured in Dulbecco's Minimal Essential Medium Eagle's (DMEM), supplemented with 10% v/v foetal bovine serum, 1% v/v L-glutamine, 1% v/v nonessential amino acid, 1% v/v penicillin/streptomycin. For drug permeability studies the cells were seeded at a density of 2×10^5 cells/well on Transwell® inserts (12-well plates) and for drug accumulation studies, Caco-2 cells were seeded at 4×10^4 cells/well cell density in 48-well plates. These cells were provided with fresh growth mediums three times a week until the time of use. Caco-2 cells were used at 21-28 days of culture when they presented a tight monolayer and expressed transport proteins [31,32].

Drug accumulation in Caco-2 cells

Drug accumulation experiments were performed using HBSS supplemented with 10 mM HEPES, buffered to pH 7.4, referred to as uptake medium. Caco-2 cells in 48-well plates were pre-incubated with uptake medium for 30 min at 37˚C and then incubated with uptake medium containing 0.1 µCi/ml ^{14}C-tenofovir, ^{14}C-dapivirine or ^{14}C-darunavir supplemented with unlabelled tenofovir, dapivirine and darunavir respectively to produce the desired concentration [33]. For inhibition studies, the inhibitor was added to the assay medium. At pre-determined intervals during the experiment, the medium was removed from the wells and at the end of the experiment the cells were washed twice with ice-cold PBS and solubilised in 1% Triton X 100 at 37°C for 30 min. The samples were mixed with 4 ml of StarScint scintillation fluid and the total radioactivity was measured using a

Beckman Coulter LS6000TA dual scintillation counter. Drug uptake was normalized to a total cellular protein content per well, which was measured using a Protein Assay kit (BCA, Sigma-Aldrich Company Ltd., Gillingham, UK), with bovine serum albumin as the standard.

Drug permeability in the Caco-2 cell monolayers

Bidirectional permeability studies were performed using confluent Caco-2 monolayers grown on Transwells [34]. The integrity of the monolayer was confirmed by measuring trans-epithelial electrical resistance (TER) before and after the experiment using an EVOM^{TM} epithelial volt-ohmmeter. The resistance of the monolayer was determined by subtracting the resistance of the solution and membrane supports from the total resistance. In this study, all cell layers used possessed a TER greater than 1250 Ω cm^2. The transport medium for the donor chamber was HBSS containing 10 mM HEPES and for the receiver chamber HBSS was supplemented with 10m M HEPES and 0.2% (w/v) Poloxamer 407. In some studies, the transport medium also contained specific transporter inhibitors or ARV drugs. All chambers were pre-incubated for 30 min with transport medium containing the appropriate inhibitor or ARV drugs to saturate any transporter binding sites. For absorptive permeability, the experiment was initiated by adding 520 µL of the relevant test solution to the apical chamber (donor chamber) of the inserts bathed with 1520 µL basolateral solution (receiver chamber). For secretory permeability, the experiment was initiated by adding 1520 µL of the relevant test solution to the basolateral chamber (donor chamber) of wells with 520 µL in the apical chamber (receiver chamber). Within 1 min, 20 µL of the test solution from both sides of chambers were removed to establish the donor concentration (C_0). Samples (200 µL) were withdrawn from the receiver chamber at 30, 60 and 90 min. The volume withdrawn was replaced with 200 µL preheated fresh transport medium, which was corrected for further calculation. After each sample, the cell layer was returned to 37˚C incubator under stirring conditions (50 rpm). After 120 min, 200 µL samples were removed from both the receiver and donor chamber. The integrity of the monolayer was confirmed by measuring the permeability of the para-cellular marker compound ^{3}H-mannitol or ^{14}C-

mannitol. Samples of medium and the cell layers at the end of the experiment were analysed using a Beckman Coulter LS6000TA dual scintillation counter, counted for 5 min per sample after addition of 4 mL of StarScint scintillation cocktail.

Drug permeability in colorectal tissue segments

All *ex-vivo* experiments were conducted with tissue derived from animals culled for different experimental purposes under the project licenses of the United Kingdom Home Office in accordance with the United Kingdom Animal Scientific Procedures Act, 1986.

Excised segments – Male Wistar guinea-pig, Male Wistar rats and Male New Zealand white rabbits were used for the *ex-vivo* drug permeability study in the colorectal tissue segments. Excision of the intestine was performed under anaesthesia and the last 10 cm of intestine was removed. The intestine was washed with cold Kreb's buffer solution and transferred to a beaker with oxygenated (95% O_2/ 5% CO_2) ice cold Kreb's buffer. All segments were cut along their mesenteric border and the muscularis externa was removed using blunt dissection while taking care to avoid Peyer's patches. The stripped colon-rectum mucosa were mounted in modified Ussing's Chamber containing oxygenated Kreb's buffer at 37°C. The effective exposed area of the tissues was 0.2 cm^2. The viability of the tissue was monitored by measuring the potential difference (PD), with values higher than -3 mV being excluded from experiment. Mannitol was included in every experiment as an integrity marker in addition to electrical monitoring.

The apparent permeability coefficient (P_{app}) for all compounds was determined in three independent experiments. The tissue was allowed to recover for 30 min, bathed bilaterally with 0.35 ml of Kreb's and continuously gassed with 95% CO_2/5% O_2 at pH 7.4 and maintained at 37 °C. The experiments were initiated by removing Krebs buffer solution from both sides and placing drug-containing medium in the donor side and drug-free medium in the receiver side. Samples of 20 µl were removed from both the receiver and donor compartments of each chamber at t=0 min. At 15 min intervals, 100 µl samples were taken from the receiver side and replaced with fresh Kreb's

buffer. At the end of the experiment (t=60 min), samples were again taken from both the donor and receiver chambers. Drug analysis was performed using liquid scintillation.

Data Analysis

In-vitro experiments using Caco-2 cells were performed on at least three independent occasions using cells of different passage. In an individual experiment, each data point represents measurements from three cell layers. *Ex-vivo* experiments using colorectal tissue segments were performed on at least three independent experiments. Statistical significance was assessed by using GraphPad Prism® (version 5.01 for Microsoft Windows, Graph Pad Software, San Diego, CA, U.S.A.). Standard one-way analysis of variance (ANOVA) was used to compare TER readings (before and after transport studies) and mean values for apparent permeability (secretory to absorptive efflux). To compare absorptive, secretory and intracellular concentrations in the presence of inhibitors to the control condition (no inhibitor), a one-way ANOVA with Dunnett's post-test was used and considered significant for p value ≤ 0.05.

In permeability experiments P_{app} was calculated according to equation 1:

$$P_{app}=dQ/dt \times (1/C_0.A) \qquad \text{Equation 1.}$$

Where dQ/dt is the gradient of the slope of flux versus time (μmoles/s), C_0 is the initial drug concentration applied in the donor chamber (μmoles/cm^3) and A is the surface area of the Transwell® filter (cm^2).

Drug permeability was measured in apical-to-basolateral (absorptive) and basolateral-to-apical (secretory) directions to enable the efflux ratio (ER) to be determined as the quotient of the secretory and the absorptive permeability according to equation 2:

$$ER= P_{app}(B\text{-}A)/P_{app}(A\text{-}B) \qquad \text{Equation 2.}$$

Where P_{app}(A-B) is the apparent permeability coefficient for absorptive drug permeability and P_{app} (B-A) is the apparent permeability coefficient for secretory drug permeability.

3. Results

Molecular docking with P-glycoprotein

To screen for the molecular interactions between the P-gp transporter and tenofovir, dapivirine and darunavir, docking studies were performed with both blind (Smina molecular docking) and knowledge-based method (GOLD molecular docking) as a preliminary screen. The crystal structure of the P-gp transporter has been reported by Aller and co-workers, which allowed us to dock the structures of tenofovir, dapivirine and darunavir against the P-gp structure [22]. Blind Smina molecular docking showed the best probable binding sites of the ligands to the P-gp protein structure. The binding energy was calculated for each confirmation and was ranked and scored to give an estimation of the binding affinity between the compound and the target.

Mannitol and digoxin were used as negative and positive control molecules, respectively, to confirm the reliability of the model to calculate binding affinity between compounds and the P-gp structure. Mannitol showed a very weak binding affinity towards the P-gp structure (-3.1 to -5.6 kcal/mol), and digoxin demonstrated a very strong binding affinity of -9.5 to -12.5 kcal/mol. Dapivirine and darunavir had preferred binding sites in the hydrophobic transmembrane domains and nucleotide binding domains with strong binding affinities of -5.1 to -8.1 kcal/mol and -6.8 to -9.8 kcal/mol, respectively (Figure 1). Tenofovir showed weak binding affinity to the P-gp structure, similar to mannitol, with an affinity of -2.5 to -5.4 kcal/mol (Figure 1).

GOLD molecular docking recognized the best 10 orientations for dapivirine and darunavir binding into the two SMINA- located binding sites of the hydrophobic transmembrane domains and nucleotide binding domains (data not shown). The scoring function was used to rank binding conformations and the binding affinity was calculated for each pose. The types of binding interactions to the specific domains were characterized for the best pose in each system by Accelrys Discovery Studio 4.5. Mannitol and digoxin showed the best confirmation towards transmembrane domain with binding affinities of -5.6 and 12.5 kcl/mol, respectively. Dapivirine's best conformation

was in hydrophobic transmembrane domains, with a binding affinity of -8.1 kcal/mol, although tenofovir and darunavir showed a binding affinity towards the nucleotide binding domains with -5.4 and -9.8 kcal/mol, respectively.

Molecular dynamics simulation of drug-P-gp interaction

Molecular dynamics simulations were performed for darunavir and dapivirine to investigate the interactions between the compounds and the P-gp transporter in detail. The relative binding free energy for mannitol and digoxin controls showed very good correlation to the molecular docking data (data not shown). Following 50 ns MD simulations for dapivirine and darunavir, MM-PBSA/MM-GBSA calculations were carried out as post analysis to calculate the relative binding free energy for the ligand-protein complexes (Table 1). The energy for Dapivirine-P-gp and Darunavir-P-gp complexes were -38.24 and -36.84 kcal/mol, respectively.

Dapivirine created 14 binding interactions with the P-gp efflux pump structure, involving close contact with Phe-692 and Ser-693 (Figure 2), creating strong conventional hydrogen bonds. Additionally, the compound formed strong carbon-hydrogen bonds with Gly-686 and Ser-693. Darunavir was found to create several strong binding interactions with the P-gp structure, including very strong conventional hydrogen bonds with Tyr-274 and Met-913 (Figure 2).

Permeability in Caco-2 cell monolayers

TER was measured before and after transport experiments with an acceptance criteria of deviation of <15% from the initial value (1650 ± 120 Ω cm^2) to ensure that epithelial barrier function was maintained [35]. Furthermore, the integrity of the cell monolayer was confirmed by the concomitant measurement of the permeability of the paracellular marker, mannitol, which had a mean absorptive P_{app} = 0.18 ± 0.04 × 10^{-6} cm/s and ER = 1.05 ± 0.22 across all experiments, in accordance with previously reported findings [32].

The absorptive and secretory permeability of tenofovir, dapivirine and darunavir was studied across Caco-2 cell monolayers over a range of concentrations (Figure 3). Tenofovir permeability in Caco-2 cell monolayers was not significantly different to that measured for mannitol. The absorptive and secretory permeabilities of tenofovir over the concentration range of 0.1 - 100 μM were P_{app} = 0.15 ± 0.04 × 10^{-6} cm/s and 0.10 ± 0.02 × 10^{-6} cm/s, respectively (Figure 3a). Recovery of tenofovir in experiments was 96.18 ± 1.75 % of the initial concentration and the drug associated with the cell layer was 0.63 ± 0.16% (Table 2).

Measurement of dapivirine permeability in the standard Caco-2 system was unreliable, caused by poor recovery of the compound (<54 %). The addition of Poloxamer 407 (0.2% w/v) in the receiver compartment improved recovery to >89% and allowed the permeability of dapivirine over the concentration range of 0.1 to 10 μM to be measured in the absorptive and secretory direction (Table 2 and Figure 3b). Poloxamer 407 0.2% w/v did not interfere with efflux pump transporters or tightness of monolayer, as demonstrated by unchanged findings for the control compounds; digoxin and mannitol (data not shown). The absorptive and secretory permeability of 10 μM dapivirine was 30.2 ± 3.8 × 10^{-6} cm/s and 38.2 ± 12.7 × 10^{-6} cm/s, respectively, with ER = 1.3 (Figure 3b). Dapivirine transport was concentration independent and >25% was recovered from the Caco-2 cells at the end of experiments (Table 2). As the drugs were quantified by scintillation counting, the data reported above reflect the sum of applied drug, tenofovir or dapivirine, plus any phosphorylated metabolites produced by the actions of cellular kinases.

Trans-epithelial transport of darunavir (10 μM) in Caco-2 cell monolayers was 6-fold greater in secretory direction compared to the absorptive direction. The absorptive and secretory permeability of darunavir across the Caco-2 cell monolayer was 6.4 ± 0.9 × 10^{-6} cm/s and 40.4 ± 3.5×10^{-6} cm/s, respectively. Over the concentration range 0.1 to 100 μM, absorptive permeability of darunavir increased from 5.9 x 10^{-6} to 7.4 x 10^{-6} cm/s while secretory permeability fell from 41.3 x 10^{-6} to 29.4 x 10^{-6} cm/s (Figure 3c), resulting in a concomitant fall in ER ranging from 7.0 to 4.0.

Effect of ABC transporter inhibitors

In order to identify any influence of the transporters in tenofovir, dapivirine and darunavir transport, the effect of several inhibitors on ARV drug permeability and cell accumulation were investigated. P-gp inhibitors included GF120918 (IC_{50} 0.3μM), verapamil (IC_{50} 2.1 μM), CsA (IC_{50} 1.3 μM) and the selective inhibitor for P-gp, haloperidol (IC_{50} 39 μM). The multidrug resistance-associated protein 2 (MRP2) inhibitor bromosulphthalein (IC_{50} 31 μM) was also included. The permeability and cell accumulation of tenofovir and dapivirine were unaffected by GF120918, haloperidol, CsA, verapamil and bromosulphthalein (Figure 4). However, considerable concentration dependent increases in absorptive flux and decreases in secretory flux of darunavir (10 μM) were observed in the presence of P-gp inhibitors, including verapamil, CsA and GF120918 (Figure 4e). Strong modulation of absorptive and secretory transport of darunavir (10 μM) was observed even at the lowest concentration of selective P-gp transporter inhibitor GF120918 (0.1 μM), which significantly reduced ER from 6.3 to 1.8 ± 0.2. Haloperidol had moderate infuence on darunavir transport and only the highest concentration, 50 μM, decreased significantly the secretory permeability, reducing the ER to 2.1 ± 0.1. All tested concentrations of the MRP-2 inhibitor (bromosulphthalein) showed a modest but significant increase only in absorptive darunavir permeability, whereas the highest concentration of bromosulphthalein (50 μM) had significant effect on bidirectional transport of compound, decreasing ER to 4.1 ± 0.4. The role of Ko 143 (BCRP inhibitor) on darunavir bidirectional transport was also investigated and there was no modulation on the transport observed.

Effects of inhibitors on cellular accumulation of the antiretroviral drugs concorded with the permeability data. Intracellular accumulation of tenofovir and dapivriene was unaffected by the presence of the P-gp inhibitors, CsA, verapamil, haloperidol and GF120918 or MRP-2 inhibitor bromosulphthalein. Darunavir uptake in Caco-2 cells after 30 min of incubation with CsA (10 μM) was enhanced by 3.6-fold, however at a lower concentration of CsA (0.01 μM) did not affect cellular

accumulation. Verapamil 0.01 μM had moderate effect on darunavir cell uptake, whereas higher concentration of 10 μM significanly enhanced accumulation by 1.8-fold. Incubation with GF120918 concentrations of 0.1 and 1 μM increased darunavir accumulation inside Caco-2 cells by almost 2-fold and 3-fold, respectively. Darunavir cell accumulation in the presence of MRP-2 inhibitor at concentration of 75 μM was enhanced by 1.8-fold, whereas a lower concentration had no effect. Darunavir cell uptake was concentration dependent and was completely abolished at a temperature of 4°C.

Co-administrations of ARV drugs

To explore the potential for drug-drug interaction between tenofovir, dapivirine and darunavir when formulated in double or triple combinations, the effect of each drug combination on permeability was evaluated over a range of concentrations (0.001 – 100 μM). Co-administrations did not significantly alter the absorptive or secretary permeability of tenofovir, dapivirine or darunavir across Caco-2 cell monolayers or alter the intracellular accumulation by Caco-2 cells when co-administered (data not shown).

Permeability in colorectal tissue segments.

To verify findings in Caco-2 cells, *ex-vivo* colorectal tissue segments of rats, guinea pigs and rabbits were used to measure tenofovir and darunavir permeability in the absence and presence of P-gp inhibitor GF120918 and co-administration with ARV drug across different species. The permeability of the para-cellular marker mannitol was measured concomitantly to confirm that the barrier function of the mucosa was maintained over the course of the experiments. Potential difference of the tissue segments was also measured as a marker of tissue viability. The absorptive permeability of tenofovir in guinea-pig, rat and rabbit colorectal mucosal segments was not influenced by the P-gp inhibitor, GF120918 (1 μM) or darunavir (100 μM), demonstrating that tenofovir is passively transported (Figure 5a). Co-administration of GF120918 1 μM with darunavir produced a significant decrease in darunavir efflux ratio in Caco-2 cells from 6.3 ± 0.9 to 1.4 ± 0.4 and a very similar effect

was obtained in rabbit colorectal intestine tissue segments with decreased efflux ratio from 4.9 ± 1.0 to 1.9 ± 0.6 (Figure 5b). Similar results were obtained for guinea-pig and rat. However, darunavir permeability in absorptive and secretory directions in both models did not significantly change in the presence of tenofovir, suggesting that there are no drug-drug interactions between these two drugs in terms of drug permeability. Due to the limitations in solubility and recovery of dapivirine in the tissue segment model, the apparent permeability in absorptive and secretory directions could not be determined.

4. Discussion

The development of effective next-generation colorectal topical microbicides has focused recently on combination-based microbicides. Combining two or more antiretroviral drugs with different mechanisms of action provides a better chance of protection, and fewer possibilities of developing resistant strains [1]. However, many of the classes of ARV proposed for use in combination are transporter substrates, raising the possibility of drug-drug interaction. The importance of drug transporters in cell and tissue compartments and their role in the disposition of antiretroviral drugs is increasingly being recognised [19]. Drug-drug interactions have been reported between PIs and NRTIs commonly combined as first line HAART agents. Co-administration of protease inhibitors such as darunavir, atazanvir, lopinavir/ritonavir with tenofovir disoproxil fumarate results in a 25-37% increase in tenofovir disoproxil fumarate exposure. *In-vitro* studies suggest that this results primarily from interaction with the P-gp transporter [19]. It is known that many PIs and NNRTIs agents can induce or inhibit P-gp transporters. Clinical studies have shown that ritonavir increases the bioavailability and plasma exposure of darunavir (14-fold), atazanavir (2.4-fold) and it is recommended as a boosting agent with all protease inhibitors [37]. In this study we combined *in-silico* and *in-vitro* experimental approaches to study any interactions of tenofovir, dapivirine and darunavir.

Blind molecular docking showed strong binding affinities to the P-gp transporter for dapivirine (-5.1 up to -8.1 kcal/mol) and darunavir (-6.8 up to -9.8), which was confirmed by GOLD molecular

docking showing that dapivirine had the highest binding affinity (-8.1 kcal/mol) towards the hydrophobic transmembrane domain. *In vitro* transport studies in cell and tissue models demonstrated clearly that darunavir was a substrate for p-glycoprotein, but unexpectedly no effect of transporters on dapivirine transport was observed in any of the biological models. The stability of binding and relative binding free energy were investigated through 50 ns MD stimulation and the results confirmed the findings of the molecular docking study. The free energy of binding was found to be higher for dapivirine (ΔG_{PB}=-38.24 ± 3.20) than for darunavir (ΔG_{PB}=-36.84 ± 2.31), suggesting stronger interactions between dapivirine and the P-gp transporter.

A possible explanation for the absence of active transport of dapivirine in Caco-2 cell monolayers is that rapid passive diffusion and escape to the cytosol provides a high accumulation of the drug inside the cell bypassing binding to P-gp within the cell plasma membrane [38 39]. It has been reported that the functional implications of the P-gp efflux transporter in biological barriers depend not only on compound binding affinity (e.g. hydrogen bonding potential, polar surface area, rotatable bond count) towards the transporter structure but also on the interplay between transmembrane passive transport rate and compounds absorptive flux and transport route across cell layers [40 41]. However, given that cell uptake studies also failed to show an influence of P-gp on dapivirine, another plausible explanation is that dapivirine exhibited a false positive prediction in the *in-silico* model. Dapivirine has a more complex chemical structure compared to the digoxin (positive control) and the resolution of the P-gp crystal structure (4.35 Å) used for computational modelling may impose limitations. High resolution of X-ray structure, < 1.50 Å, is likely to produce more accurate docking results, whereas low resolution with values greater than 2.50 Å might lead to errors in docking and simulations.

A comparison of transporter gene expression at the human colorectum with different colorectal cell lines, including SW837, SW1463, HRA-16, shows that the Caco-2 cell line, which is routinely used to study human intestinal drug permeability, is also the most suitable model for the study of colorectal drug transport [18]. The permeability of tenofovir in this model was low, similar to permeability of

mannitol (used as a paracellular marker) and equivalent in absorptive and secretory directions. The ER and cellular uptake of tenofovir did not show any significant difference in the presence of P-gp and MRP-2 specific inhibitors. These results were in agreement with findings reported by Ray and co-workers [42] and Neumanova and co-workers [43], suggesting that this agent traverses the mucosa via the paracellular route and is not a substrate of any transporters expressed in Caco-2 cells. This observation concorded with the results of the computational study using blind molecular docking and GOLD molecular docking showing very weak binding affinity (-2.5 up to -5.4 kcal/mol) towards the P-gp efflux pump transporter.

Our results contradict the reported absorptive permeability of dapivirine in Caco-2 cell monolayers of $3.28 \pm 0.16 \times 10^{-6}$ cm/s [40] and $2.14 \pm 0.81 \times 10^{-6}$ cm/s [41]. We found that P_{app} values for dapivirine were critically dependent on drug recovery, which when improved from 55% to >89% in Caco-2 cell model changed P_{app} from $2.9 \pm 0.9 \times 10^{-6}$ cm/s to $34.2 \pm 0.31 \times 10^{-6}$ cm/s. In the unexpected absence of P-gp activity on dapivirine transport discussed above, the high permeability of dapivirine was attributed to passive diffusive transport enabled by the drug's lipophilicity, log P= 5.29 (Figure 3). For darunavir, a significant difference ($p<0.001$) was observed between absorptive vs. secretory permeability in Caco-2 cell monolayers. The permeability of darunavir reduced over the concentration range studied (0.1-100 µM), indicating that the active transport component became saturated. P-gp inhibitors such as verapamil and GF120918 significantly reduced initial ER of darunavir 10 µM from 6.3 to 1.2. Although these inhibitors are not completely selective, the influence of P-gp in darunavir efflux across Caco-2 cell monolayers can be deduced from the absence of any effect of Ko 143 which rule out an effect of BCRP, and the weak effect of bromosulphthalein which indicates that MRP 2 plays a minor role. In uptake studies using subconfluent Caco-2 cells in 96-well plates, darunavir efflux was inhibited by CsA 10 µM and GF120918 1 µM, increasing intracellular concentration of darunavir by more than 200% compared to the control. In the presence of bromosulphthalein, darunavir concentration increased by 75% compared to the control. These results clearly demonstrate P-gp and to a lesser extent MRP2-mediated transport of darunavir in

Caco-2 cells, albeit without using the more selective Pg-p inhibitor PSC833 (valspodar) to rule out an effect of BCRP. Darunavir has previously been identified as a P-gp substrate in Caco-2 cells with bi-directional transport rates being strongly concentration-dependent [44] and the involvement of MRP-2 in the transport of darunavir being suggested [45].

Drug permeability was also measured in guinea-pig, rat and rabbits colorectal mucosal segments using dual chamber transport system. Tissue models offer many advantages over *in-vitro* methods, such as a preserved microenvironment at the mucosal membrane, multicellularity, and regional differences in the expression of drug transporters. Dapivirine permeability could not be determined reliably in the *ex-vivo* model because of low recovery of drug in experiments, but data for the permeability of tenofovir (100 µM) and darunavir (10 µM) was consistent across all three species and confirmed the findings observed in Caco-2 cell model. In rabbits, the species most commonly used to study topical microbicides, the secretory permeability of darunavir was inhibited by GF120918 (ER from 4.9 ± 1.0 to 1.9 ± 0.6).

5. Conclusion

The effect of co-administering the antiretroviral drugs is necessary in order to determine any possible drug-drug interactions of biopharmaceutical relevance. In experimental models, tenofovir and dapivirine did not interact with P-gp, MRP2 or BCRP transporters, whereas darunavir was shown to be a substrate of P-gp and MRP2. Experiments using rat, rabbit and guinea-pig colorectal tissue segments confirmed that tenofovir was passively transported, being concentration independent and unaffected by transporter inhibitors, but showed that darunavir transport was strongly affected by P-gp transporter in the colorectal mucosa. The mechanism of transport and interactions with ABC-efflux pump transporters concorded across all *in-vitro* and *in-silico* models for tenofovir and darunavir. Interestingly, dapivirine permeability was determined not to be P-gp dependent, despite *in-silico* data suggesting that it is a substrate, thus further demonstrating the need of experimental validation for *in silico* predictions, a tenet that is generalizable for drug discovery programs. This is an

aspect that warrants further investigation. When administered in combination, the disposition of the proposed triple-therapy antiretroviral drugs in the colorectal mucosa will depend on their distinctly different permeability, but was not interdependent.

Acknowledgments

We thank members of the MOTIF consortium for useful exchange of ideas and discussions during the course of the study. We thank Janssen R&D Ireland for provision of darunavir and Gilead Sciences for provision of tenofovir. This work was supported by the European Union's Seventh Framework Programme for research, technological development and demonstration under grant agreement No 305316 as part of the MOTIF (Microbicide Optimization through Innovative Formulation for vaginal and rectal delivery) project.

References:

(1) Herrera, C.; Cranage, M.; McGowan, I.; Anton, P.; Shattock, R. J. Colorectal Microbicide Design: Triple Combinations of Reverse Transcriptase Inhibitors Are Optimal against HIV-1 in Tissue Explants. *AIDS* **2011**, *25* (16), 1971–1979.

(2) Grulich, A. E.; Zablotska, I. Commentary: Probability of HIV Transmission through Anal Intercourse. *Int. J. Epidemiol.* **2010**, *39* (4), 1064–1065.

(3) Baggaley, R. F.; White, R. G.; Boily, M.-C. HIV Transmission Risk through Anal Intercourse: Systematic Review, Meta-Analysis and Implications for HIV Prevention. *Int. J. Epidemiol.* **2010**, *39* (4), 1048–1063.

(4) Fletcher, P. S.; Elliott, J.; Grivel, J.-C.; Margolis, L.; Anton, P.; McGowan, I.; Shattock, R. J. Ex Vivo Culture of Human Colorectal Tissue for the Evaluation of Candidate Microbicides. *AIDS* **2006**, *20* (9), 1237–1245.

(5) McGowan, I. Rectal Microbicide Development. *Curr. Opin. HIV AIDS* **2012**, *7* (6), 526–533.

(6) Herrera, C.; Cranage, M.; McGowan, I.; Anton, P.; Shattock, R. J. Reverse Transcriptase Inhibitors as Potential Colorectal Microbicides. *Antimicrob. Agents Chemother.* **2009**, *53* (5), 1797–1807.

(7) Shattock, R. J.; Rosenberg, Z. Microbicides: Topical Prevention against HIV. *Cold Spring Harb. Perspect. Med.* **2012**, *2* (2), a007385.

(8) Rosenberg, Z. F.; Devlin, B. Future Strategies in Microbicide Development. *Best Pract. Res. Clin. Obstet. Gynaecol.* **2012**, *26* (4), 503–513.

(9) Kiser, P. F.; Mahalingam, A.; Fabian, J.; Smith, E.; Damian, F. R.; Peters, J. J.; Katz, D. F.; Elgendy, H.; Clark, M. R.; Friend, D. R. Design of Tenofovir-UC781 Combination Microbicide Vaginal Gels. *J. Pharm. Sci.* **2012**, *101* (5), 1852–1864.

(10) Krakower, D. S.; Mayer, K. H. Pre-Exposure Prophylaxis to Prevent HIV Infection: Current

Status, Future Opportunities and Challenges. *Drugs* **2015**, *75* (3), 243–251.

(11) Schader, S. M.; Oliveira, M.; Ibanescu, R.-I.; Moisi, D.; Colby-Germinario, S. P.; Wainberg, M. A. In Vitro Resistance Profile of the Candidate HIV-1 Microbicide Drug Dapivirine. *Antimicrob. Agents Chemother.* **2012**, *56* (2), 751–756.

(12) Pham, P. A.; Gallant, J. E. Tenofovir Disoproxil Fumarate for the Treatment of HIV Infection. *Expert Opin. Drug Metab. Toxicol.* **2006**, *2* (3), 459–469.

(13) Malcolm, R. K.; Woolfson, A. D.; Toner, C. F.; Morrow, R. J.; McCullagh, S. D. Long-Term, Controlled Release of the HIV Microbicide TMC120 from Silicone Elastomer Vaginal Rings. *J. Antimicrob. Chemother.* **2005**, *56* (5), 954–956.

(14) Nel, A.; Smythe, S.; Young, K.; Malcolm, K.; McCoy, C.; Rosenberg, Z.; Romano, J. Safety and Pharmacokinetics of Dapivirine Delivery from Matrix and Reservoir Intravaginal Rings to HIV-Negative Women. *J. Acquir. Immune Defic. Syndr.* **2009**, *51* (4), 416–423.

(15) Romano, J.; Variano, B.; Coplan, P.; Roey, J. Van; Douville, K.; Rosenberg, Z.; Temmerman, M.; Verstraelen, H.; Bortel, L. Van; Weyers, S.; Mitchnick, M. Safety and Availability of Dapivirine (TMC120) Delivered from an Intravaginal Ring. **2009**.

(16) Tremblay, C. L. Combating HIV Resistance - Focus on Darunavir. *Ther. Clin. Risk Manag.* **2008**, *4* (4), 759–766.

(17) Englund, G.; Rorsman, F.; Rönnblom, A.; Karlbom, U.; Lazorova, L.; Gråsjö, J.; Kindmark, A.; Artursson, P. Regional Levels of Drug Transporters along the Human Intestinal Tract: Co-Expression of ABC and SLC Transporters and Comparison with Caco-2 Cells. *Eur. J. Pharm. Sci.* **2006**, *29* (3-4), 269–277.

(18) Mukhopadhya, I.; Murray, G. I.; Berry, S.; Thomson, J.; Frank, B.; Gwozdz, G.; Ekeruche-Makinde, J.; Shattock, R.; Kelly, C.; Iannelli, F.; Pozzi, G.; El-Omar, E. M.; Hold, G. L.; Hijazi, K. Drug Transporter Gene Expression in Human Colorectal Tissue and Cell Lines: Modulation with Antiretrovirals for Microbicide Optimization. *J. Antimicrob. Chemother.* **2016**, *71* (2), 372–386.

(19) Kis, O.; Robillard, K.; Chan, G. N. Y.; Bendayan, R. The Complexities of Antiretroviral Drug-Drug Interactions: Role of ABC and SLC Transporters. *Trends Pharmacol. Sci.* **2010**, *31* (1), 22–35.

(20) Volpe, D. A. Application of Method Suitability for Drug Permeability Classification. *AAPS J.* **2010**, *12* (4), 670–678.

(21) Giacomini, K. M.; Huang, S.-M.; Tweedie, D. J.; Benet, L. Z.; Brouwer, K. L. R.; Chu, X.; Dahlin, A.; Evers, R.; Fischer, V.; Hillgren, K. M.; Hoffmaster, K. A.; Ishikawa, T.; Keppler, D.; Kim, R. B.; Lee, C. A.; Niemi, M.; Polli, J. W.; Sugiyama, Y.; Swaan, P. W.; Ware, J. A.; Wright, S. H.; Yee, S. W.; Zamek-Gliszczynski, M. J.; Zhang, L. Membrane Transporters in Drug Development. *Nat. Rev. Drug Discov.* **2010**, *9* (3), 215–236.

(22) Aller, S. G.; Yu, J.; Ward, A.; Weng, Y.; Chittaboina, S.; Zhuo, R.; Harrell, P. M.; Trinh, Y. T.; Zhang, Q.; Urbatsch, I. L.; Chang, G. Structure of P-Glycoprotein Reveals a Molecular Basis for Poly-Specific Drug Binding. *Science* **2009**, *323* (5922), 1718–1722.

(23) Nissink, J. W. M.; Murray, C.; Hartshorn, M.; Verdonk, M. L.; Cole, J. C.; Taylor, R. A New Test Set for Validating Predictions of Protein-Ligand Interaction. *Proteins* **2002**, *49* (4), 457–471.

(24) Darden, T.; York, D.; Pedersen, L. Particle Mesh Ewald: An N·log(N) Method for Ewald Sums in Large Systems. *J. Chem. Phys.* **1993**, *98* (12), 10089.

(25) Ryckaert, J.-P.; Ciccotti, G.; Berendsen, H. J. . Numerical Integration of the Cartesian Equations of Motion of a System with Constraints: Molecular Dynamics of N-Alkanes. *J. Comput. Phys.* **1977**, *23* (3), 327–341.

(26) Case, D. A.; Cheatham, T. E.; Darden, T.; Gohlke, H.; Luo, R.; Merz, K. M.; Onufriev, A.; Simmerling, C.; Wang, B.; Woods, R. J. The Amber Biomolecular Simulation Programs. *J. Comput. Chem.* **2005**, *26* (16), 1668–1688.

(27) Sitkoff, D.; Sharp, K. A.; Honig, B. Accurate Calculation of Hydration Free Energies Using Macroscopic Solvent Models. *J. Phys. Chem.* **1994**, *98* (7), 1978–1988.

(28) Wang, W.; Kollman, P. A. Free Energy Calculations on Dimer Stability of the HIV Protease Using Molecular Dynamics and a Continuum Solvent Model. *J. Mol. Biol.* **2000**, *303* (4), 567–582.

(29) Weiser, J.; Shenkin, P. S.; Still, W. C. Approximate Atomic Surfaces from Linear Combinations of Pairwise Overlaps (LCPO). *J. Comput. Chem.* **1999**, *20* (2), 217–230.

(30) Tsui, V.; Case, D. A. Theory and Applications of the Generalized Born Solvation Model in Macromolecular Simulations. *Biopolymers 56* (4), 275–291.

(31) Sun, H.; Chow, E. C.; Liu, S.; Du, Y.; Pang, K. S. The Caco-2 Cell Monolayer: Usefulness and Limitations. *Expert Opin. Drug Metab. Toxicol.* **2008**, *4* (4), 395–411.

(32) Hubatsch, I.; Ragnarsson, E. G. E.; Artursson, P. Determination of Drug Permeability and Prediction of Drug Absorption in Caco-2 Monolayers. *Nat. Protoc.* **2007**, *2* (9), 2111–2119.

(33) Kis, O.; Zastre, J. A.; Hoque, M. T.; Walmsley, S. L.; Bendayan, R. Role of Drug Efflux and Uptake Transporters in Atazanavir Intestinal Permeability and Drug-Drug Interactions. *Pharm. Res.* **2013**, *30* (4), 1050–1064.

(34) Lakeram, M.; Lockley, D. J.; Sanders, D. J.; Pendlington, R.; Forbes, B. Paraben Transport and Metabolism in the Biomimetic Artificial Membrane Permeability Assay (BAMPA) and 3-Day and 21-Day Caco-2 Cell Systems. *J. Biomol. Screen.* **2007**, *12* (1), 84–91.

(35) Briske-Anderson, M. J.; Finley, J. W.; Newman, S. M. The Influence of Culture Time and Passage Number on the Morphological and Physiological Development of Caco-2 Cells. *Exp. Biol. Med.* **1997**, *214* (3), 248–257.

(36) Artursson, P.; Karlsson, J. Correlation between Oral Drug Absorption in Humans and Apparent Drug Permeability Coefficients in Human Intestinal Epithelial (Caco-2) Cells. *Biochem. Biophys. Res. Commun.* **1991**, *175* (3), 880–885.

(37) HIV/AIDS Guidelines - adultandadolescentgl.pdf

http://aidsinfo.nih.gov/contentfiles/lvguidelines/adultandadolescentgl.pdf.

(38) Raub, T. J. P-Glycoprotein Recognition of Substrates and Circumvention through Rational Drug Design. *Mol. Pharm.* **2006**, *3* (1), 3–25.

(39) Desai, P. V; Sawada, G. A.; Watson, I. A.; Raub, T. J. Integration of in Silico and in Vitro Tools for Scaffold Optimization during Drug Discovery: Predicting P-Glycoprotein Efflux. *Mol. Pharm.* **2013**, *10* (4), 1249–1261.

(40) Al-Jayyoussi, G.; Price, D. F.; Francombe, D.; Taylor, G.; Smith, M. W.; Morris, C.; Edwards, C. D.; Eddershaw, P.; Gumbleton, M. Selectivity in the Impact of P-Glycoprotein upon Pulmonary Absorption of Airway-Dosed Substrates: A Study in Ex Vivo Lung Models Using Chemical Inhibition and Genetic Knockout. *J. Pharm. Sci.* **2013**, *102* (9), 3382–3394.

(41) Varma, M. V. S.; Panchagnula, R. Enhanced Oral Paclitaxel Absorption with Vitamin E-TPGS: Effect on Solubility and Permeability in Vitro, in Situ and in Vivo. *Eur. J. Pharm. Sci.* **2005**, *25* (4-5), 445–453.

(42) Ray, A. S.; Cihlar, T.; Robinson, K. L.; Tong, L.; Vela, J. E.; Fuller, M. D.; Wieman, L. M.; Eisenberg, E. J.; Rhodes, G. R. Mechanism of Active Renal Tubular Efflux of Tenofovir. *Antimicrob. Agents Chemother.* **2006**, *50* (10), 3297–3304.

(43) Neumanova, Z.; Cerveny, L.; Ceckova, M.; Staud, F. Interactions of Tenofovir and Tenofovir Disoproxil Fumarate with Drug Efflux Transporters ABCB1, ABCG2, and ABCC2; Role in Transport across the Placenta. *AIDS* **2014**, *28* (1), 9–17.

(44) Lachau-Durand, S.; Annaert, P.; Steemans, K.; Willems, B.; Mannens, G.; Raoof, A.; Meuldermans, W. Transport Characteristics of the HIV Protease Inhibitor Darunavir (TMC114) in Caco-2 Monolayers.

(45) Fujimoto, H.; Higuchi, M.; Watanabe, H.; Koh, Y.; Ghosh, A. K.; Mitsuya, H.; Tanoue, N.; Hamada, A.; Saito, H. P-Glycoprotein Mediates Efflux Transport of Darunavir in Human Intestinal Caco-2 and ABCB1 Gene-Transfected Renal LLC-PK1 Cell Lines. *Biol. Pharm. Bull.*

2009, *32* (9), 1588–1593.

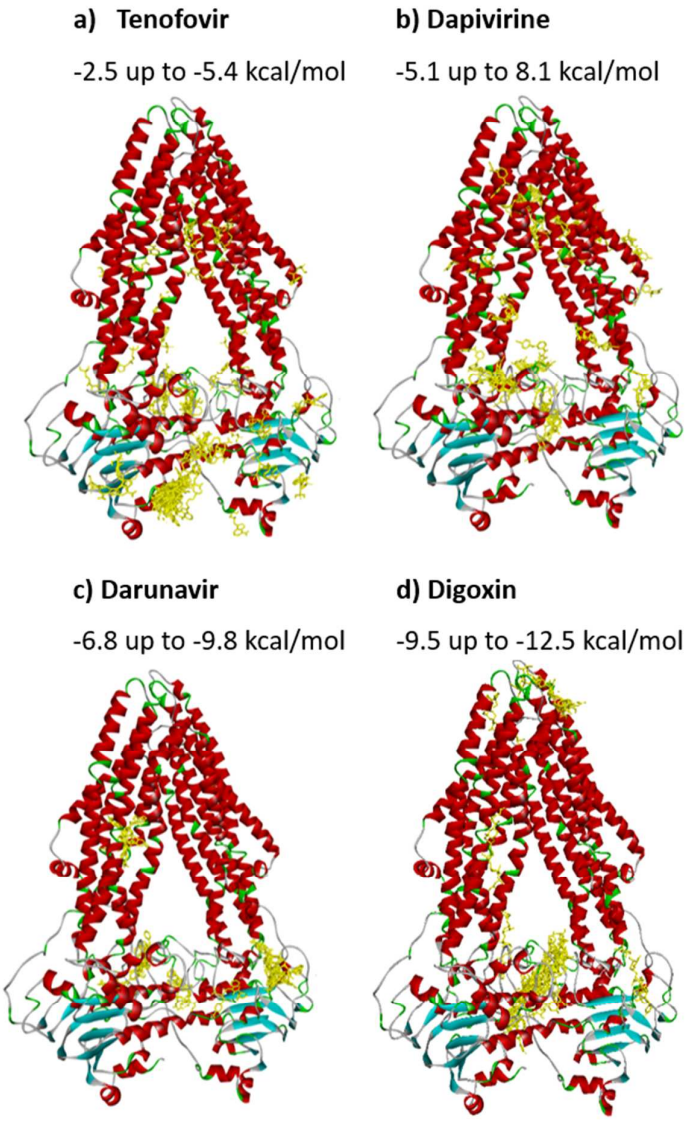

Figure 1. Docking of tenofovir, dapivirine, darunavir and digoxin (positive control) shown in yellow colour to a P-gp efflux pump. The ranges of energy represent the affinities for corresponding ligand-protein structures.

Table 1. Average energy contributions to form of dapivirine and darunavir complexes with P-gp.

Complex	Dapivirine (kcal/mol)	Darunavir (kcal/mol)
ΔE_{ele}	-12.90 ± 1.84	-22.36 ± 2.13
ΔE_{vdw}	-55.54 ± 1.56	-59.73 ± 2.57
ΔE_{sol}	30.20 ± 2.22	45.25 ± 3.35
ΔG_{PB}	-38.24 ± 3.20	-36.84 ± 2.31
ΔG_{GB}	-52.13 ± 2.68	-45.71 ± 2.19

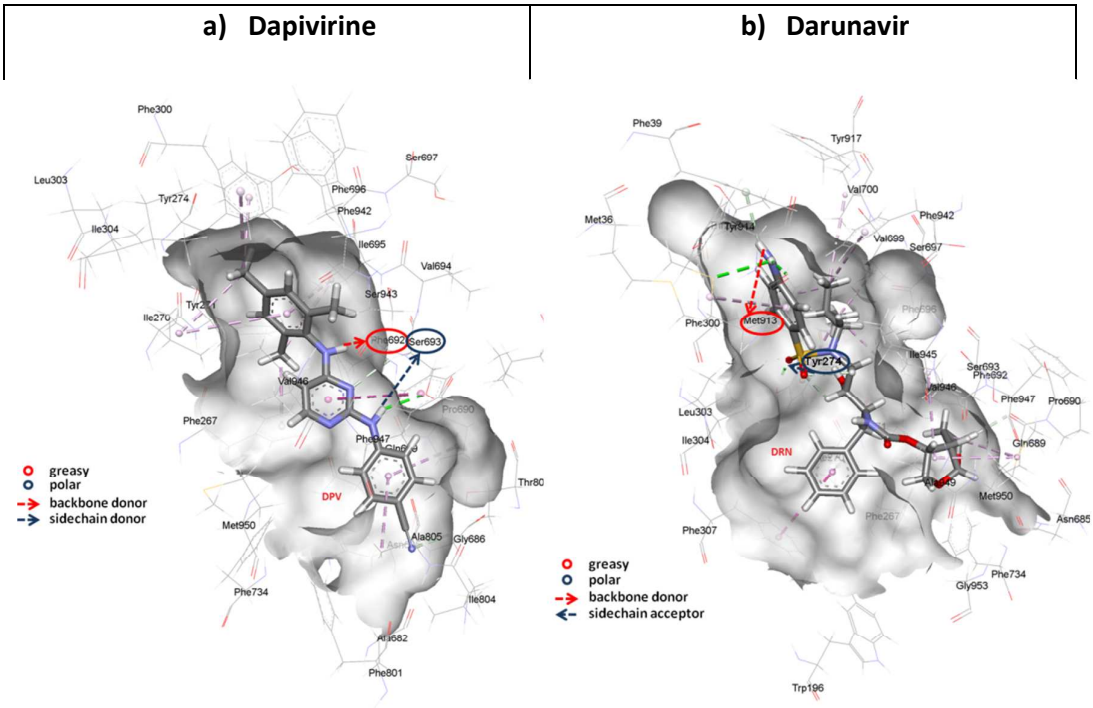

Dapivirine	Distance (Å)	Types	Darunavir	Distance (Å)	Types
:DPV1240:H - :PHE692:O	1.88	Conventional Hydrogen Bond	:TYR274:HH - :DRN1240:O2	1.91	Conventional Hydrogen Bond
:DPV1240:H1 - :SER693:OG	2.44	Conventional Hydrogen Bond	:DRN1240:H4 - :MET913:SD	2.92	Conventional Hydrogen Bond
:GLY686:HA2 - :DPV1240:N1	2.88	Carbon Hydrogen Bond	:DRN1240:H4 - :MET913:O	2.19	Conventional Hydrogen Bond
:SER693:HA - :DPV1240:N	2.70	Carbon Hydrogen Bond	:DRN1240:H29 - :GLN689:O	2.44	Carbon Hydrogen Bond

Figure 2. Drug - P-gp transporter complexes in the transmembrane domain after MD simulation and the most important interactions determined by the 50 ns molecular simulation (a) dapivirine, (b) darunavir.

Table 2. Recovery of ARVs after 2 h absorptive permeability assays in Caco-2 cell monolayers (total recovery and recovery from the basolateral side, i.e. receiver chamber, and cell monolayer). Data represent mean ± SD, n=3.

			Recovered compound (%)	
Compound	**Concentration (µM)**	**Total recovery (%)**	**Receiver compartment**	**Caco-2 cell monolayer**
Tenofovir	100	96.18 ± 1.75	1.14 ± 0.05	0.63 ± 0.16
Dapivirine	10	86.50 ± 5.10	45.96 ± 5.27	25.91 ± 2.53
Darunavir	10	98.38 ± 3.66	9.71 ± 1.07	1.52 ± 0.30

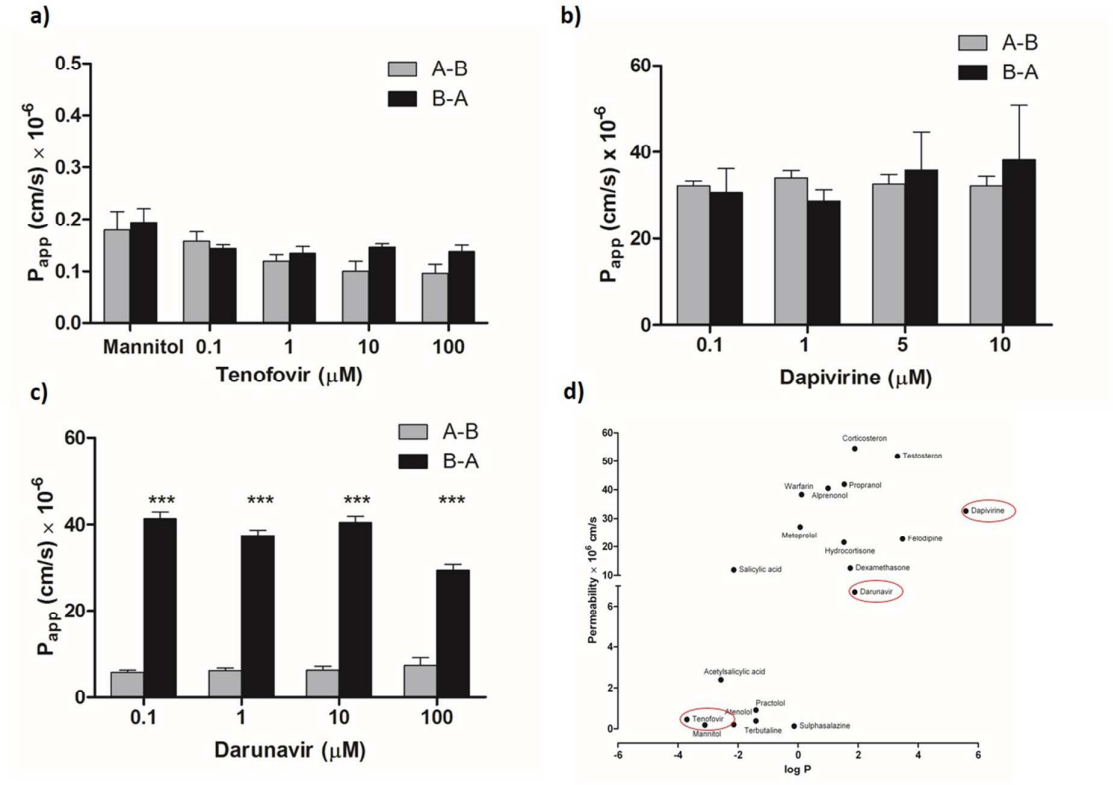

Figure 3. Antiretroviral drug permeability. Concentration dependence of the absorptive (grey bars) and secretory (black bars) permeability in Caco-2 cells of a) tenofovir 0.1 – 100 μM, b) dapivirine 0.1 – 10 μM, and c) darunavir 0.1 – 100 μM. Data represent mean ± SD from three independent studies, each performed in triplicate. d) the absorptive P_{app} of tenofovir, darunavir and dapivirine in the context of reported P_{app} of drugs in Caco-2 monolayers in similar experiments as a function of octanol-water partition coefficients [36].

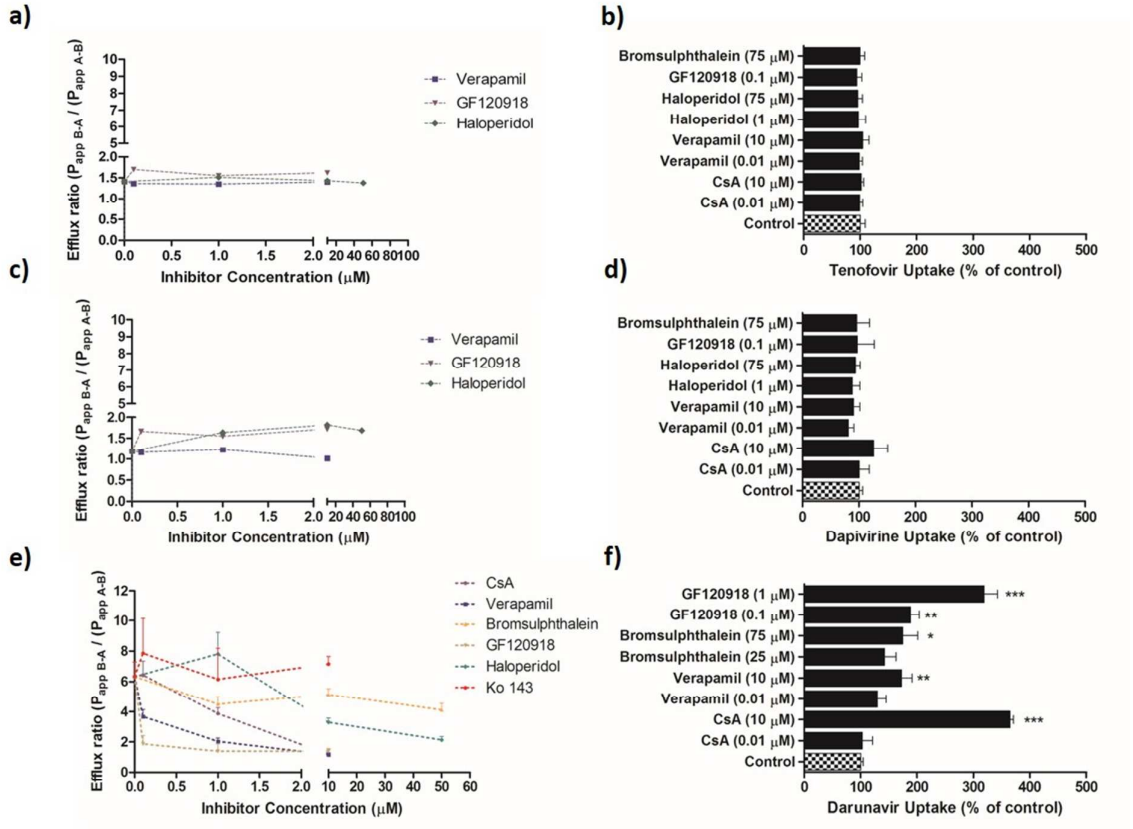

Figure 4. Influence of transporter inhibitors on drug permeability and cell uptake. The effect of inhibitors on the efflux ratio of (a) [^{14}C] tenofovir (100 μM), (c) [^{14}C] dapivirine (10 μM), (e) [^{14}C] darunavir (10 μM) in Caco-2 cell monolayers. Effect of transporter inhibitors on the accumulation of b) tenofovir (100 μM) d) dapivirine (10 μM) and f) darunavir (10 μM) by Caco-2 cells in 48-well plates. Data represent mean ± SEM from three independent studies each performed with six replicates per data point (*** $p<0.001$; ** $p<0.01$; * $p<0.05$). Note: error bars are within the data points.

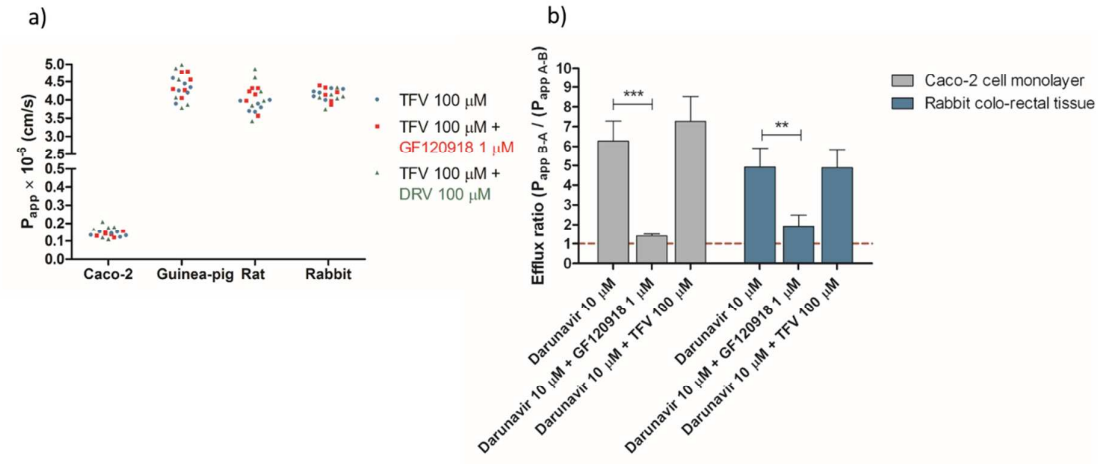

Figure 5. Permeability in colorectal tissue segments. (a) Absorptive permeability of tenofovir (100 µM) in Caco-2 cell monolayer and guinea-pig, rat and rabbit colorectal mucosal segments. (b) Efflux ratio of darunavir 10 µM in the presence of P-gp inhibitor GF120918 1 µM and tenofovir (TFV) 100 µM across rabbit excised colorectal mucosal segments. Data represent mean ± SD from three independent experiments (*** $p<0.001$; ** $p<0.01$).

Graphical abstract

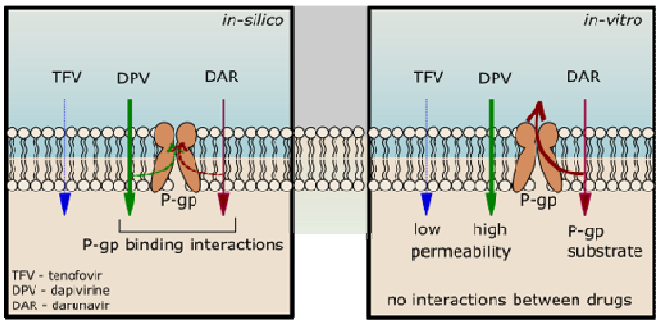

For Table of contents only